J Fluoresc (2016) 26:1151–1159
DOI 10.1007/s10895-016-1824-1

FLUORESCENCE NEWS ARTICLE

Influence of Shell Formation on Morphological Structure, Optical and Emission Intensity on Aqueous Dispersible NaYF4:Ce/Tb Nanoparticles

Anees A. Ansari[1] · A. K. Parchur[2] · B. Kumar[2] · S. B. Rai[2]

Received: 17 January 2016 / Accepted: 9 May 2016 / Published online: 20 May 2016

Abstract A highly water-dispersible $NaYF_4$:Ce/Tb (core), $NaYF_4$:Ce/Tb@$NaYF_4$(core/shell) and $NaYF_4$:Ce/Tb@$NaYF_4$@SiO_2 (core/shell/SiO_2) nanoparticles (NPs) were synthesized via a general synthesis approach. The growth of an inert $NaYF_4$ and silica shell (~14 nm) around the core-NPs resulted in an increase of the average size of the nanopaticles as well as broadening of their size distribution. The optical band-gap energy slightly decreases after shell formation due to the increase the crystalline size. To optimize the influence of shell formation a comparative analysis of photoluminescence properties (excitation, emission, and luminescence decay time) of the core, core/shell, and core/shell/SiO_2 NPs were measured. The emission intensity was significantly enhanced after inert shell formation around the surface of the core NPs. The Commission International de l'Eclairage chromaticity coordinates of the emission spectrum of core, core/shell, core/shell/SiO_2 NPs lie closest to the standard green color emission at 545 nm. By quantitative spectroscopic measurements of surface-modified core-NPs, it was suggested that encapsulation with inert and silica layers was found to be effective in retaining both luminescence intensity and dispersibility in aqueous environment. Considering the high aqueous dispersion and enhanced luminescence efficiency of the core-NPs make them an ideal luminescent material for luminescence bioimaging and optical biosensors.

Keyword Luminescent NPs · Optical absorbance · Band gap energy · Photoluminescence · Decay time

Introduction

Recently, synthesis of luminescent nanomaterials (NMs) has been focused by many researchers for their applications in biomedical imaging, optical bioprobes, photonics, nanophosphors, and therapeutics [1–5]. A large number of luminescent NMs have been reported in the literature such as traditional organic dyes (Rhodamine, Fluorescein iso-thiocyanate), quantum dots (CdS, CdSe, CdTe, ZnS, ZnO) [4, 5], metal NPs (Au, Ag, Ru etc.), and lanthanide (Ln^{3+}) ions doped NMs are widely used in the field of biological analyses [3–9]. However, these luminescent nanomaterials have not been extensively used as optical bioprobes because they have drawbacks such as weak photostability, broad absorption and emission bands, low dispersion in water, toxicity, blinking properties, and moderate quantum yield. In order to address these key issues, it is a challenge to develop alternative luminescent NMs, which have better characteristics as compared to conventional luminescent NMs. To overcome this problem, Ln^{3+} ion doped NPs have been recently reported [10–17]. Such kind of Ln^{3+} ion doped luminescent NMs exhibit unique luminescent properties, such as sharp absorption and emission bands, high quantum yields, long lifetimes, superior photostability, low cytotoxicity, and excellent biocompatibility [10]. These features are particularly attractive as potential emitters for the fluorescent biolabeling of biomacromolecules

Electronic supplementary material The online version of this article (doi:10.1007/s10895-016-1824-1) contains supplementary material, which is available to authorized users.

✉ Anees A. Ansari
aneesaansari@gmail.com

[1] King Abdullah Institute for Nanotechnology, King Saud University, Riyadh -11451, Saudi Arabia

[2] Department of Physics, Banaras Hindu University, Varanasi -221005, India

at ambient temperature and therefore require a further development of new luminescent materials possessing a high surface area and which are optically active [13–17].

Among various host materials, rare-earth fluoride host (ex. $NaYF_4$) NMs doped with Yb^{3+}/Er^{3+}, Yb^{3+}/Tm^{3+}, Yb^{3+}/Ho^{3+} have been extensively studied because these upconversion luminescent materials possesses advantageous properties such as high refractive index, low phonon energy (~350 cm^{-1}), and more stable physical and chemical properties [18]. On the other hand, certain Ln^{3+} ions doped $NaYF_4$ NPs show down-conversion emission under deep UV excitation, which has significant technological implications in different field of material sciences as well as biological sciences such as biolabeling, optical bioprobes, and detection of biological analytes [19–21]. Moreover, these Ln^{3+} ions doped NPs show tunable multicolor emissions by varying the Ln^{3+} ion concentrations in the host NPs. In addition, tunable multicolor emission using a single excitation wavelength is highly suitable for multiplexed biological detection applications [19–22]. Recently, Tu et al., synthesized amine functionalized Ce^{3+}/Tb^{3+}-doped $NaYF_4$ NPs and utilized as a new type time resolved Förster resonance energy transfer for optical bio-probe applications [20]. Chen et al., reported multicolor emission achieved via co-doping with Ce^{3+}/Tb^{3+} ions [19]. Wu et al. [23] Ghose et al. [21] and Kim et al. [24] also reported the luminescent properties of Ce^{3+}/Tb^{3+} ions doped $NaYF_4$ NPs under UV excitation. However, due to the non-radiative decay from the defects on the surface of the NPs, the luminescence efficiency of nanostructural materials is usually lower than that of the corresponding bulk materials. To reduce these defects, the growth of an inert crystalline shell around the core-NPs to form core/shell architecture has been regarded as an effective strategy to improve the luminescent efficiency [17, 25]. In recent years, we and some other research groups were successfully applied this strategy to synthesis core/shell architecture, in which luminescent Ln^{3+} ions were doped in core (active) and inert host compounds as shells [17, 25]. This inert inorganic crystalline shell efficiently passivates the fast non-radiative decay channels originating from the surface states of the NPs. Although, growth of an inert shell around core-NPs enhances the radiative decay rate still toxicity of the NPs is a significant concern to the biological systems. Hence, much work has to be done to modify and/or functionalize the surface of NPs. A simple but effective method is to grow an amorphous silica shell around the NPs, forming the so-called core/shell nanostructures [13, 17]. The silica coating can improve the photo-stability and biocompatibility of the NPs, due to the presence of –OH bonds on the surface of the NPs. It is well established method for conjugation of biomolecules to a silica surface [13].

In this paper, we developed a solution based soft chemical synthesis method for the preparation of highly water dispersible Ce^{3+} and Tb^{3+} co-doped $NaYF_4$ luminescent core-NPs. The growth of $NaYF_4$ shell surrounding the core-NPs was created to improve the luminescence efficiency by enhancing the energy transfer from Ce^{3+} to Tb^{3+} ions. The core/shell nanostructures represent one approach that has been researched to increase the luminescence efficiency by removing surface quenching sites that can strongly quench the RE^{3+} luminescence. Transmission electron microscopy (TEM) micrographs and different spectroscopic methods were utilized to investigate the crystalinity, size, and shape of the nanostructured materials. The excitation, emission, and luminescent decay time of the NPs were studied. Also, the surface of the core/shell NPs was modified with amorphous silica to enhance the dispersion ability of the NPs. Moreover, the formation of amorphous silica surface is easy to conjugate with various biomolecules and shows excellent dispersion ability in aqueous solvents, good biocompatible and non-toxic in nature. Thus, such a configuration of the NPs can satisfy the desired criteria of high luminescence as well as long-life, easy conjugation, dispersions in water, and photo-stability in the development of a biolabiling application. In this core/shell/SiO_2 nanoparticles, the SiO_2 shell and $NaYF_4$:Ce/Tb@$NaYF_4$ core/shell will interact with each other, which affects emission properties of the core/shell/SiO_2 nanoparticles. However, its physical nature has not been well understood. Therefore, it is necessary to deeply study the effect of surface coating or relationship of inert crystalline $NaYF_4$ and SiO_2 shell on structural, optical and photoluminescence properties of Ce^{3+} and Tb^{3+} ions doped $NaYF_4$:Ce/Tb nanoparticles. These new core/shell/SiO_2 NPs show a great potential to be used as a luminescent bio-probe for the detection of biological analytes and biolabiling applications etc.

Experimental

Materials

Yttrium oxide (99 %, BDH, England), Terbium oxide (99.99 %, Alfa Aesar, Germany), Cerium nitrate (99.99 %, BDH Chemicals Ltd., England), Sodium fluorite(NaF), Ethylene-diamine tetra-acetic acid(EDTA), Tetraethyl orthosilicate (TEOS, 99 wt% analytical reagent A.R.), C_2H_5OH, NaOH, HNO_3 and NH_4OH were used as the starting materials without any further purification. Yttrium nitrate ($Y(NO_3)_3.6H_2O$) and terbium nitrate ($Tb(NO_3)_3.6H_2O$) hexa-hydrated were prepared by dissolving the corresponding oxides in diluted nitric acid. Nanopure water was used for preparation of the solutions. Ultrapure de-ionized water was prepared using a Milli-Q system (Millipore, Bedford, MA, USA). All other chemicals used were of reagent grade.

Preparation of $NaYF_4$:Ce/Tb NPs

For the preparation of $NaYF_4$:Ce^{3+}/Tb^{3+} NPs, 1.379, 0.091, and 0.090 g of $Y(NO_3)_36H_2O$, $Ce(NO_3)_36H_2O$ and $Tb(NO_3)_36H_2O$, respectively were dissolved together in 100 mL dist. Water and heated up to 80 °C. An equivalent amount 1:1 M ratio of EDTA (1.631 g) was dissolved in dist. Water (50 mL) and introduced dropwise in metal solution for complex formation. This reaction continued up to 2 h for complex formation. Afterward, another solution was formed as dissolving the 1:3 M ratio of sodium fluorite (0.518 g) in minimum quantity of distilled water. This solution was mixed up in this forgoing reaction and kept for constant stirring with heating (80 °C) on hot plate for 1 h [15]. The reaction mixture was heated up to 150 °C for 3 h under reflux conditions until a white precipitate was formed. The synthesized NPs were then collected by centrifugation, washed with distilled water and absolute ethanol five times, and then dried in oven at 60 °C for 6 h for further characterization.

Preparation of $NaYF_4$:Ce/Tb@$NaYF_4$ Core/Shell NPs

In the procedure of $NaYF_4$:Ce^{3+}/Tb^{3+}@$NaYF_4$ core/shell NPs formation, similar EDTA based complexation process was used as discussed above. Initially, 0.399 g of $NaYF_4$: Ce^{3+}/Tb^{3+} NPs were dispersed in 10 mL of distilled water with the help of ultrasonic bath and then constant stirring for 30 min. Typically 0.632 g $Y(NO_3)_36H_2O$ was dissolved in distilled water and then a solution of EDTA was injected into this reaction. Afterward, sodium fluorite (0.410 g) dissolved in distilled water was mixed-up in this foregoing mixed system, and the suspension was refluxed at 150 °C for 3 h until the precipitation was occurred. This white precipitate was centrifuged and washed five times with ethanol to remove of excess of unreacted reactants. The core/shell NPs were collected after centrifugation and then dried in oven at 60 °C for 6 h for further characterization.

Preparation of Silica Coated $NaYF_4$:Ce/Tb@$NaYF_4$@SiO_2 Core/Shell NPs

The $NaYF_4$:Ce^{3+}/Tb^{3+}@$NaYF_4$@SiO_2 core/shell NPs were prepared through a versatile Stober sol-gel process as described below [13, 26]. The synthesized $NaYF_4$:Ce^{3+}/Tb^{3+}@$NaYF_4$ NPs (50 mg) were well dispersed in a mixed solution of deionized water (50 mL), ethanol (70 mL) and concentrated aqueous ammonia (1.0 mL) in a three-neck round-bottom flask. Afterward, 1.0 mL of tetraethyl orthosilicate (TEOS) was added slowly for hydration, and the reaction was allowed to proceed for 5–6 h under continuous mechanical stirring. After 6 h of continuous stirring at room temperature, the silica-coated core/shell NPs were separated by centrifugation, washed five times with ethanol then dried in oven at 60 °C for 6 h for further characterization.

Characterization

The size and morphology of the samples were inspected using a field emission transmission electron microscope (FE-TEM) equipped with the EDX (FETEM, JEM-2100F, JEOL, Japan) operating at an accelerating voltage of 200 kV. EDX analysis was used to confirm the presence of the elements. The samples for TEM were prepared by depositing a drop of a colloidal ethanol solution of the powder sample onto a carbon-coated copper grid. Fourier transform infrared spectroscopy (FTIR) spectra were recorded on a Perkin-Elmer 580B IR spectrometer using KBr pellet technique in the range 4000–400 cm^{-1}. The UV/Vis absorption spectra were measured in the Perkin-Elmer Lambda-40 spectrophotometer in the range 190–600 nm, with the sample contained in 1 cm^3 stoppered quartz cell of 1 cm path length. Photoluminescence excitation spectra of the samples were recorded using Hitachi F-4500 spectrometer equipped with a 150 W Xe lamp as a source having spectral resolution of 3 nm. Photoluminescence spectra were studied by a 266 nm pulsed Nd-YAG laser (Spitlight 600, Innolas, Germany) source. Photoluminescence decay was recorded with an Edinburgh instrument F-920 equipped with a 100 W μs flash xenon lamp as the excitation source. All measurements were performed at room temperature.

Results and Discussion

Crystallographic Studies

Phase purity and crystal structure of the core, core/shell and silica coated core/shell/SiO_2 NPs were characterized by XRD analysis (Scheme 1). In Fig. 1, all the diffraction peaks of the core and core/shell NPs are broad with low intensity can be exclusively indexed as a pure cubic phase of $NaYF_4$, the location and relative intensities of the reflection planes coincide well with the literature values (JCPDS card No. 77–2042) and no impurity phase can be found in the diffraction pattern, indicating that pure α-$NaYF_4$ phase was obtained under this condition [19]. It is found that the widths of all reflection planes are broader due to small crystalline size of the nanomaterials. As illustrated in Fig. 1, the relative diffraction peak intensity of core/shell/SiO_2 NPs decrease in respect to core and core/shell NPs, because amorphous silica surface coating significantly influence the grain size, resulting the reflection intensity is changed in XRD pattern. Whereas, we did not observed any characteristic peak of amorphous silica in XRD pattern of core/shell/SiO_2 NPs may be due to thinner layer of silica encapsulated around the surface of NPs.

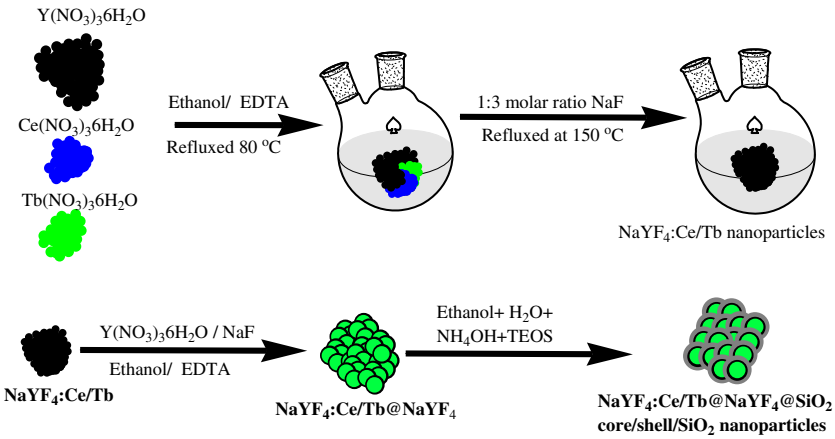

Scheme 1 Schematic diagram showing the synthesis process of core, core/shell and silica surface modified core/shell/SiO2 NPs

Morphological Studies

TEM was employed to determine the size and morphology changes after surface modifications of the NPs. Figure 2. shows the low resolution TEM images of core and silica coated core/shell/SiO_2 NPs. As shown in Fig. 2a, core-NPs are irregular spherical, highly agglomerated, polycrystalline with a narrow size distribution ranging from 10 to 15 nm. The high aggregation and irregular shape may be due to the employed complexation rout of core-NPs, in that case little amount of EDTA has remained attached around the surface of core-NPs. The existence of EDTA is also confirmed by FTIR observations see in Fig. 3. Inset of Fig. 2a shows the selected area electron diffraction pattern (SAED) of the core NPs. The SAED pattern shows a continuous circular ring patterns with bright diffraction spots shows the highly crystalline nature of the core-NPs. It is worth noting that after amorphous silica surface modification the morphology, size and polydispersibility of the core/shell NPs is greatly affected. It indicates that silica has been grafted successfully surrounding the core/shell NPs as seen in Fig. 2b & c. It can be seen that the core/shell NPs are composed of well dispersed and irregular spherical particles with average diameter around 20 nm (Fig. 2c). The luminescent cores are dark and an irregular shape whereas, silica surface is in light grey color. Interestingly, the silica coated core/shell NPs did not exhibit a smooth surface. This confirms that the irregular shape of the NPs resulted from a co-precipitation process. Such a feature is highly desirable for optical bioprobe or bioimaging applications.

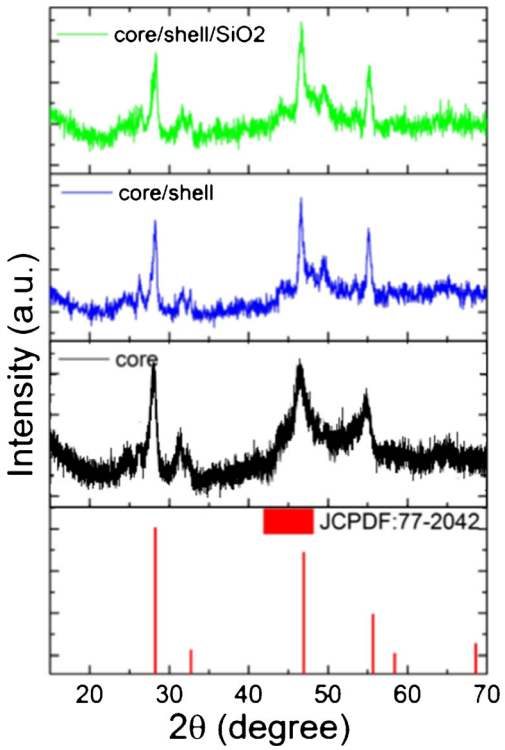

Fig. 1 X-ray diffraction pattern of core, core/shell, and core/shell/SiO2 NPs

Element composition of the synthesized samples were analysis by energy dispersive X-ray spectroscopy (EDX) to examine the successful incorporation of doping Ce and Tb ions into the $NaYF_4$ lattice (Fig. 2d & e). The presence of Si element in EDX analysis suggests that amorphous silica has been grafted effectively around the core-NPs, which provides an additional evidence for encapsulation of silica layer. Note that the C and Cu signals were from the Cu grid (substrate) on which the sample is deposited. The FE-TEM images of pure core-NPs and silica coated core/shell/SiO_2 NPs (Fig. 2e) and the EDX pattern (Fig. 2e) simultaneously show that the silica coated core/shell/SiO_2 NPs exhibit a well ordered mesoporous structure with a 2D cubic arrangement.

Optical Properties

FTIR spectroscopy was examined in order to confirm the successful silica surface modification of the core/shell NPs. A broad absorption band is observed in between 3000 and 3600 cm^{-1}, and weak intensity band located at 1622 cm^{-1} are assigned to the O–H symmetrical stretching and bending

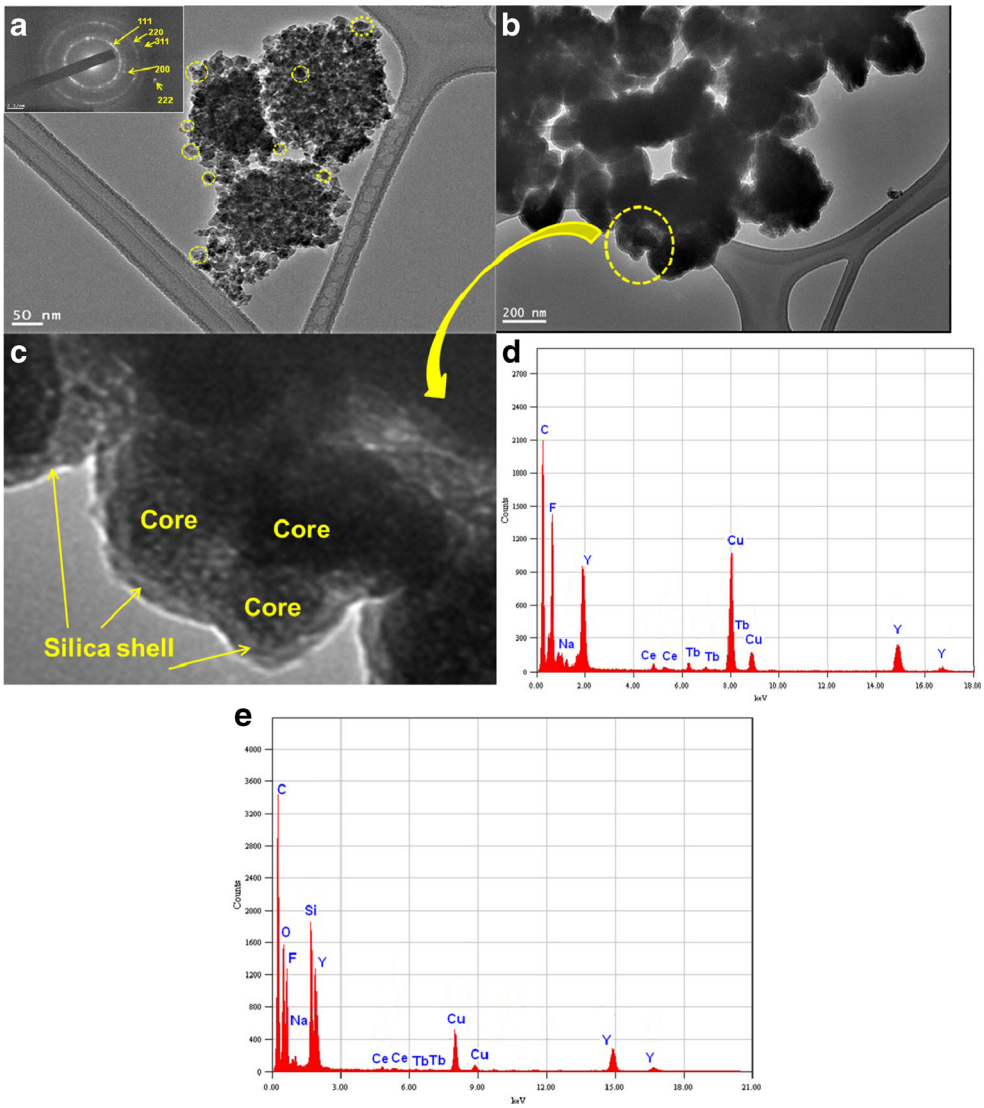

Fig. 2 TEM images of a NaYF4:Ce/Tb (core) in inset shows the SAED patterns and b NaYF4:Ce/Tb@NaYF4@SiO2 (core/ shell/SiO2) NPs. c Energy dispersive X-ray spectrograph of core and d core/shell/SiO2 NPs

vibrational modes of H_2O molecules of EDTA (Fig. 3) [13, 17, 26, 27]. The low intensity sharp peaks at 1740 and at around 1430 cm^{-1}, which can be ascribed to C = O and C–O stretching vibration of EDTA [27, 28]. The peaks at 3035 and 2881 cm^{-1} are based on the asymmetric and symmetric stretching bands of $–CH_3$. A doublet strong transmission band observed at 1080 cm^{-1} originates from the Si–O–Si asymmetric, symmetric stretching vibration of amorphous silica. The bands at 800 and 450 cm^{-1} are assigned to the Si–OH and Si–O stretching respectively [13, 17, 26]. These characteristic infrared transmission bands confirm the successful silica surface modification around the core/shell NPs.

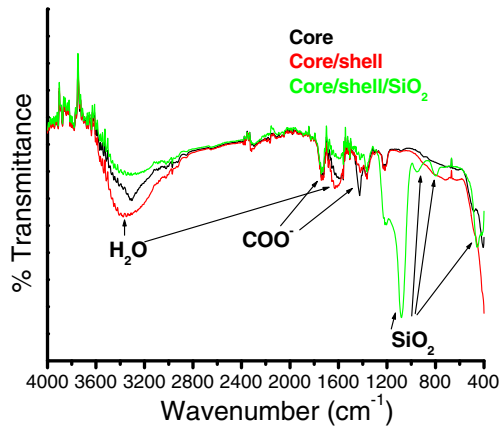

Fig. 3 FTIR spectra of core, core/shell, and core/shell/SiO2 NPs

Optical absorption spectra were used to characterize the optical features of the as-synthesized core and core/shell NPs. Figure 4 illustrates the optical absorption spectra of core, core/shell and silica coated core/shell/SiO_2 NPs measured in absolute ethanol. It is noted that the absorption spectrum of core/shell/SiO_2 NPs exhibits distinctively different shape of band in colloidal phase in the UV-region. A significant enhancement in the absorption band is due to the silica surface modification, which enhanced the surface properties of NPs

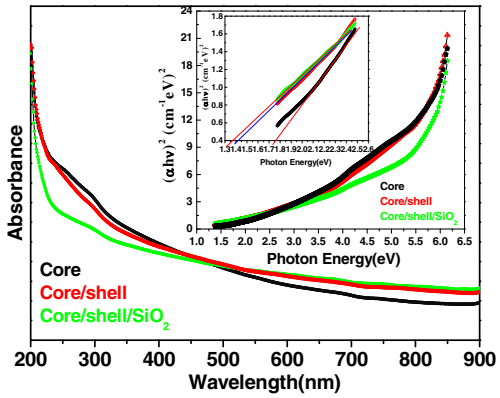

Fig. 4 UV-vis absorption spectra of a core b core/shell and c core/shell/SiO2 NPs suspended in absolute ethanol; inset shows the plot of $(\alpha h\upsilon)2$ vs. photon energy($h\nu$) of the a core b core/shell and c core/shell/SiO2 NPs

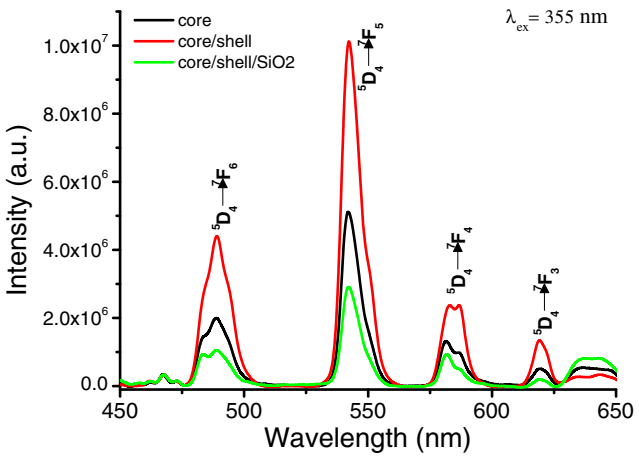

Fig. 6 Emission spectra of the as-prepared core, core/shell and core/shell/SiO2 NPs

[15–17]. These observations indicate the successfully encapsulation of amorphous silica layer around the surface of bare NPs. Optical energy band gap, E_g for the core, core/shell and core/shell/SiO_2 NPs are determined from the sharply increasing absorption region according to Tauc and Menth's law [29]. The inset of Fig. 4 shows a plot of ($\alpha h\nu$) versus the photon energy ($h\nu$). The experimentally estimated band gap is about 1.75, 1.41 and 1.36 eV, for core, core/shell and core/shell/SiO_2 NPs, respectively. It is worth mentioning that the band gap energies are decreasing after surface modification because of increase crystalline size of the materials [17]. The optical behavior of Ce^{3+} and Tb^{3+} ions doped core-NPs with doping concentrations of 5 % is investigated because these ions are good probes for the chemical environment of the Ln^{3+} ions. Ln^{3+} ions doped in the unit cell will replaced by Y^{3+} ions. In this context photoluminescence properties of the NPs were investigated by excitation, emission and lifetime measurement at room temperature as shown in Figs. 5–7. The excitation spectra was taken with a monitoring wavelength of 541 nm, and emission spectra was excited on 355 nm. As shown in Fig. 5, all three samples display several excitation peaks monitored at 317($^7F_6 \rightarrow {}^5D_0$), 326($^7F_6 \rightarrow {}^5D_1$), 340($^7F_6 \rightarrow {}^5L_8$), 350($^7F_6 \rightarrow {}^5D_{10}$ & $^5G_5$), 368($^7F_6 \rightarrow {}^5G_6$), and 377($^7F_6 \rightarrow {}^5D_3$) nm are originating from 4*f*–4*f* transitions of Tb^{3+} ions along with strong band located at 275 nm correspond to 4*f*–5*d* transition of Ce^{3+} ions [16, 25]. The excitation spectra show a similar trend in all samples and all excitation transitions are identical to the excitation of Tb^{3+} ion in powder samples [25]. As seen in Fig. 5, the peak intensities of 4*f*–4*f* transitions of Tb^{3+} ions are increase it may be related to surface growth of undoped $NaYF_4$ layer around the core-NPs. Whereas, the relatively peak intensity decrease after silica surface modification, due to the influence of amorphous silica.

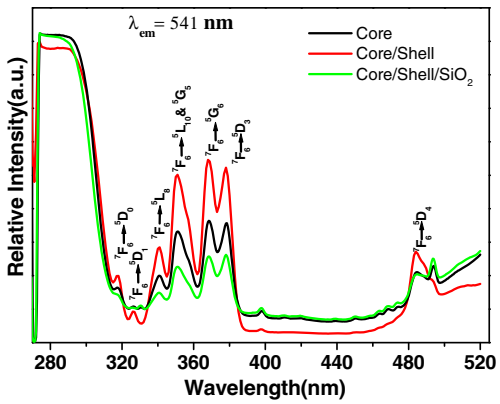

Fig. 5 Excitation spectra of core, core/shell, and core/shell/SiO2 NPs

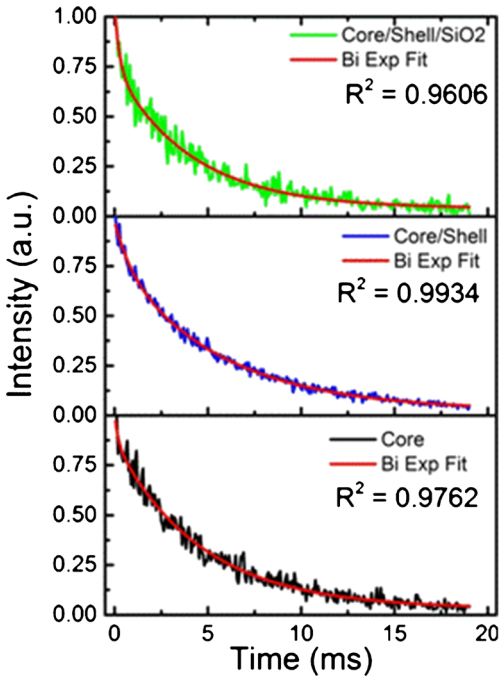

Fig. 7 Photoluminescence decay curves of core, core/shell, and core/shell/SiO2 NPs at λex = 355 nm and λem = 541 nm fitted using biexponential decay equations

The emission spectra of three samples were measured from 450 to 750 nm are mainly composed of six strong peaks located at 488 nm($^5D_4 \rightarrow {}^7F_6$), 541 nm ($^5D_4 \rightarrow {}^7F_5$), 583 nm ($^5D_4 \rightarrow {}^7F_4$), 618 nm ($^5D_4 \rightarrow {}^7F_3$), 640 nm ($^5D_4 \rightarrow {}^7F_2$), and 674 nm ($^5D_4 \rightarrow {}^7F_1$), which separately correspond to the characteristic 4*f*–4*f* transitions of Tb^{3+} ions and in good agreement with the standard energy levels [16, 25]. Among the Tb^{3+} emission transitions, the most intense and sharp emission band is observed at 541 nm due to the $^5D_4 \rightarrow {}^7F_5$ transition reveals greatest sensitivity in all three samples [16, 25]. This emission transition is the true fingerprint for the characteristic emission lines corresponding to the 4*f*–4*f* transition of the Tb^{3+} ion, which is induced by the change in the chemical environment of the Tb^{3+} ions during the formation of a new chemical bond between host and the Tb^{3+} ion [16, 24, 25]. The relative intensities and peak positions of all emission transitions are in consistent with the previously literature reports, indicating that the Ce^{3+} and Tb^{3+} ion are co-doped in a $NaYF_4$ crystal site [19, 20]. Moreover, shape and intensity of transitions provide a better model to investigate the effect of environment on optical properties of the NPs. As seen in Fig. 6b, typical band features of all emission transitions clearly suggest the surface modification of the NPs [24, 25]. A remarkable enhancement is observed in emission intensity of inert shell coated core/shell NPs in respect to the uncoated core-NPs. This increase emission intensity may be attributed to the fact that a significant amount of non-radiative centers existing on the surface of core-NPs are eliminated by the shielding effect of the $NaYF_4$ shell [17, 25]. On the other hand, in this core/shell/SiO_2 structure, the distance between the luminescent lanthanide ions and the surface quenchers is increased, thus reducing the non-radiative pathways and suppressing the energy quenching in energy transfer processes [7, 14, 17, 25, 30, 31]. On the other hand, NPs are prepared in aqueous media and their surface may be covered by a large amount of hydroxyl groups either chemically anchored or physically adsorbed to the surface, as confirmed by the FTIR and UV/Vis study. These hydroxyl groups made them highly aqueous dispersion at room temperature. Whereas, these hydroxyl groups may also cause considerable non-radiative transition and reduce the quantum efficiency of the luminescent Ln^{3+} ions. Appearance of reduced intensity of emission transitions in core-NPs with respect to core/shell NPs clearly indicates the effect of hydroxyl groups. Notably, core/shell NPs reveals better enhancement in emission intensity most likely because the low phonon energy of the $NaYF_4$ shell that not only resist water but also minimizes resonant energy loss.

It is worth noticing that as seen in Fig. 6c, the emission intensity of silica surface modified core/shell/SiO_2-NPs is remarkably lower than the core/shell NPs, which is similar to some literatures related to silica coated nanophosphors [32–35]. And, After coating, the possible reasons of the remarkable emission intensity reductions are as follows: SiO_2 coating leads to the decrease in $NaYF_4$:Ce/Tb amount per unit volume of the sample; SiO_2 is in amorphous state and the silanol (SiO-H) group which acts as the luminescence quencher may present; the power of the excitation light reaching the $NaYF_4$:Ce/Tb core becomes weak due to the scattering and reflection of silica shell. Further, the emission of surface modified NPs was examined in terms of their Commission International de l'Eclairage coordinates (Fig. 8) and lifetime of $^5D_4$ state of Tb^{3+} ions (Fig. 7) to understand the effect of local environment on luminescence properties.

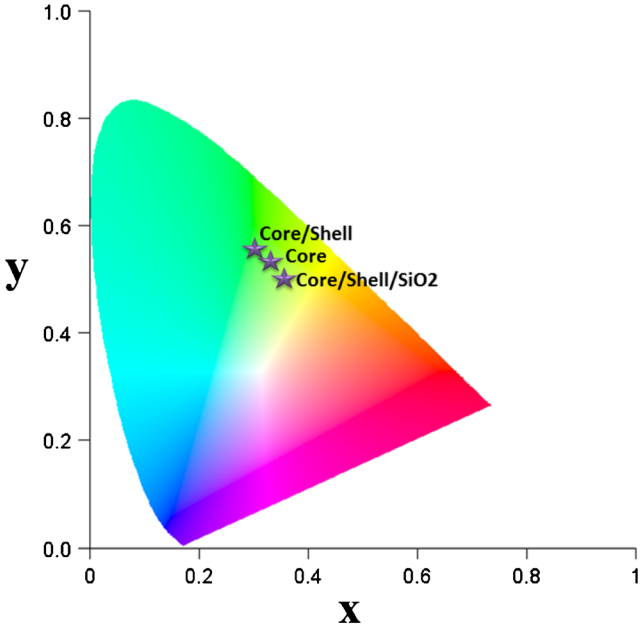

Fig. 8 CIE diagram of core, core/shell, and core/shell/SiO2 NPs

Representative photoluminescence decay time of core, core/shell and core/shell/SiO_2 NPs are illustrated in Fig. 7. Photoluminescence decay curves of $^5D_4$ (541 nm) level of Tb^{3+} ion for core, core/shell, and core/shell/SiO_2 NPs under 355 nm excitation (λ_{em} = 541 nm) is shown in Fig. 7. The decay curve for $^5D_4 \rightarrow {}^7F_5$ transition (541 nm) of Tb^{3+} ions are not well fitted with monoexponential function as $I = I_0 \exp(-t/\tau_1)$ (Fig. S1, **ESI**), where I_0 and I are the intensities at the $t = 0$ and t ms and τ is the lifetime. It is further confirmed by plotting Log(I) − t curves of the photoluminescence decay for the $^5D_4 \rightarrow {}^7F_5$ transition of Tb^{3+} ion (**ESI S1(b)**). Fitting parameters obtained after mono-exponential fitting are shown

Table 1 The lifetime parameters obtained from the biexponential fitting to the luminescence decay data of the Core, Core/Shell, and Core/Shell/SiO_2 NPs at 355 nm excitation (λ_{em} = 541 nm)

Nanoparticles	I_1(%)	τ_1(ms)	I_2(%)	τ_2(ms)	τ_{av}(ms)	R^2
Core	14.4	0.182	85.6	4.631	3.99	0.9762
Core/Shell	20.5	0.838	79.5	5.602	4.62	0.9934
Core/Shell/SiO_2	30.4	0.265	69.6	4.141	2.96	0.9606

Table S1. This is may be due to the presence of significant numbers of –OH ions, nonradiative processes, and/or surface defects present on the surface of the NPs [36]. It result the deviation mono-exponential fit to the photoluminescence decay data (poor R^2). Furthermore, the photoluminescence decay data was fitted using a biexponential function which is defined as, $I = I_1\exp(-t/\tau_1) + I_2\exp(-t/\tau_2)$, where τ_1 and τ_2 are the fast and slow components of the luminescence lifetime decay constants and I_1 and I_2 are the intensity parameters [37]. The biexponential fitting to the decay data of core, core/shell, and core/shell/SiO_2 NPs were shown in Fig. 7 and fitting parameters (I_1, τ_1, I_1, τ_2, τ_{av} and R^2) are summarized in Table 1. Where τ_{av} is the average lifetime for $^5D_4 \rightarrow {}^7F_5$ transition of Tb^{3+} ion (541 nm) is calculated using the formula as $\tau_{av} = (I_1\tau_1 + I_2\tau_2)/(I_1 + I_1)$. In general, biexponential behavior is observed due to the presence of an inhomogeneous distribution of the photoluminescent ions (Tb^{3+}) in the core/shell. For a typical biexponential fitting, under 355 nm excitation, the lifetime decay values for core and core/shell samples are found to be 182 μs (τ_1) and 4.631 ms (τ_2) with an average lifetime of 3.99 ms (τ_{av}) and core/shell samples 838 μs (τ_1) and 5.602 ms (τ_2) with an average lifetime of 4.62 ms (τ_{av}), respectively. Recently, Parchur et al. reported the lifetime value of Tb^{3+} doped $CaMoO_4$ NPs in the range of 60–896 μs [25]. Also, Li et al. reported average of lifetime value to be 8.1 ms for 900 °C annealed $SiO_2@Ca_{0.95}Tb_{0.05}MoO_4$ sample [38]. Further, lifetime values extensively depend on presence of –OH ions present on the surface of the NPs, nonradiative transition of $^5D_4 \rightarrow {}^7F_j$, and energy transfer between $^5D_4$ levels of Tb^{3+} ions. Increase in lifetime values of core/shell NPs as compared to the core-NPs was also supported by increase in luminescence by inert shell (without Tb^{3+}) formation of active core (with Tb^{3+}). Veggel and his group demonstrated that the surface modified lanthanide ion doped nanomaterials efficiently controls the non-radiative process due to the reduction in presence of dangling bond present on the surface of the NPs [38]. It results the increase in quantum yield and lifetime values of core/shell NPs as compared to core particles [39]. It is also found that, τ_1, τ_2 have a 14.4 and 85.6 % contribution in τ_{av} value in case of core particles, respectively while ~20.5 and 79.5 % contribution was found for core/shell particles. For core/shell/SiO_2 samples, the lifetime values are found to be 265 μs (τ_1) and 4.424 ms (τ_2) with an average lifetime of 2.96 ms (τ_{av}). The τ_1, τ_2 have a 30.4 and 69.6 % contribution in τ_{av} value. Moreover, the slow lifetime component τ_2 of core/shell/SiO_2 NPs lies between the value of core and core/shell NPs.

Conclusions

In conclusion, we have successfully synthesized water dispersible with greatly improve luminescent down-conversion core, core/shell and core/shell/SiO_2 NPs via facile complexation rout. FETEM and FTIR spectral analysis confirmed the core/shell/SiO_2 structure. The optical absorption band edges were shifted to longer wavelength from seed luminescent core to silica modified core/shell/SiO_2 NPs. The bandgap energy was decrease after shell formation, which attributed to the quantum-size effect due to the growth of the crystalline inert and amorphous silica layers improve the crystallinity of the core/shell nanomaterials. The formation of an inert shell before silica surface modification mainly promote luminescence enhancement and silica greatly improve their solubility character in aqueous solvents. A remarkable improvement of luminescent efficiency was achieved after grown an inert inorganic shell surrounding the surface of seed core-NPs. This novel strategy after improving the luminescence performance and water dispersibility in aqueous solvents is important for realizing practical applications in luminescent bioimaging or as optical bio-probe for detection of analytes.

Acknowledgments This work was supported through the project funded by national plan for science, technology and innovation (MAARIFAH) King Abdulaziz City for Science and Technology, Kingdom of Saudi Arabia, award Number (13-Bio1246-02).

References

1. Yuan J, Wang G, Majima K, Matsumoto K (2001) Synthesis of a terbium fluorescent chelate and its application to time-resolved fluoroimmunoassay. Anal Chem 73(8):1869–1876
2. Yang H, Santra S, Walter GA, Holloway PH (2006) GdIII-functionalized fluorescent quantum dots as multimodal imaging. Adv Mater 18(21):2890–2894
3. Ye Z, Tan M, Wang G, Yuan J (2004) Novel fluorescent europium chelate-doped silica nanoparticles: preparation, characterization and time-resolved fluorometric application. J Mater Chem 14(5): 851–856
4. Zhang C, Ji X, Zhang Y, Zhou G, Ke X, Wang H, Tinnefeld P, He Z (2013) One-pot synthesized aptamer-functionalized CdTe:Zn^{2+} quantum dots for tumor-targeted fluorescence imaging in vitro and in vivo. Anal Chem 85(12):5843–5849
5. Alivistas P (2004) The use of nanocrystal for biological detection. Nat Biotechnol 22(1):47–52
6. Reiss P, Protiere M, Li L (2009) Core/shell semiconductor nanocrystals. Small 5(2):154–168
7. Liu T, Liu B, Zhang H, Wang Y (2005) The fluorescence bioassay platforms on quantum dots nanoparticles. J Fluoresc 15(5):729–733
8. Chan WCW, Nie S (1998) Quantum dot bioconjugates for ultrasensitive nonisotopic detection. Science 281(5385):2016–2018
9. Huhtinen P, Kivela M, Kuronen O, Hagren V, Takalo H, Tenhu H, Lovgren T, Harma H (2005) Synthesis, characterization, and application of Eu(III), Tb(III), Sm(III), and Dy(III) lanthanide chelate nanoparticle labels. Anal Chem 77(8):2643–2648
10. Han S, Deng R, Xie X, Liu X (2014) Enhancing luminescence in lanthanide-doped upconversion nanoparticles. Angew Chem Int Ed 53(44):11702–11715
11. Ansari AA, Parchur AK, Alam M, Azzeer A (2014) Structural and photoluminescence properties of Tb-doped $CaMoO_4$ nanoparticles with sequential surface coatings. Mater Chem Phys 147(3):715–721

12. Wang F, Banerjee D, Liu Y, Chen X, Liu X (2010) Upconversion nanoparticles in biological labeling, imaging, and therapy. Analyst 135(8):1839–1854
13. Ansari AA, Alam M, Labis JP, Alrokayan SA, Shafi G, Hasan TN, Alshatwi AA (2011) Luminescent mesoporous $LaVO_4$:Eu^{3+} core-shell nanoparticles: synthesis, characterization, biocompatibility and their cytotoxicity. J Mater Chem 21(48):19310–19316
14. Parchur AK, Ansari AA, Singh BP, Hasan TN, Syed NA, Rai SB, Ningthoujam RS (2014) Enhanced luminescence of $CaMoO_4$:Eu core@shell nanoparticles and functionalization of Fe_3O_4-$CaMoO_4$:Eu hybrid magnetic nanoparticles for hyperthermia applications. Integr Biol 6(1):53–64
15. Ansari AA, Hasan TN, Syed NA, Labis JP, Parchur AK, Shafi G, Alshatwi AA (2013) In-vitro cyto-toxicity, geno-toxicity and bio-imaging evaluation of on-pot synthesized luminescent functionalized mesoporous SiO_2@$Eu(OH)_3$ core-shell microspheres. Nanomed: Nanotech Med & Biol 9(8):1328–1335
16. Ansari AA, Labis JP (2012) On-pot synthesis and photoluminescence properties of luminescent functionalized mesoporous SiO_2@$Tb(OH)_3$ core-shell nanospheres. J Mater Chem 22(32): 16649–16656
17. Ansari AA, Parchur AK, Alam M, Azzeer A (2014) Effect of surface coating on optical properties of Eu^{3+}-doped $CaMoO_4$ nanoparticles. Spectrochim Acta Part A 131(10):30–36
18. Tian G, Zhang X, Gu Z, Zhao Y (2015) Recent advances in upconversion nanoparticles-based multifunctional nanocomposites for combined cancer therapy. Adv Mater 27(47):7692–7712
19. Chen B, Peng D, Chen X, Qiao X, Fan X, Wang F (2015) Establishing the structural integrity of core-shell nanoparticles against elemental migration using luminescent lanthanide probes. Angew Chem Int Ed 54(43):12788–12790
20. Tu D, Liu L, Ju Q, Liu Y, Zhu H, Li R, Chen X (2011) Time-resolved FRET biosensor based on amine-functionalized lanthanide-doped $NaYF_4$ nanocrystals. Angew Chem Int Ed 50(28): 6306–6310
21. Ghosh P, Kar A, Patra A (2010) Energy transfer study between Ce^{3+} and Tb^{3+} ions in doped and core-shell sodium yttrium fluoride nanocrystals. Nanoscale 2(7):1196–1202
22. Liu Y, Tu D, Zhu H, Ma E, Chen X (2013) Lanthanide-doped luminescent nano-bioprobes: from fundamentals to biodetection. Nanoscale 5(4):1369–1384
23. Wu Y, Yang D, Kang X, Ma P, Huang S, Zhang Y, Li C, Lin J (2013) Core–shell structured luminescent and mesoporous β-$NaYF_4$:Ce^{3+}/Tb^{3+}@$mSiO_2$-PEG nanospheres for anti-cancer drug delivery. Dalton Trans 42(27):9852–9861
24. Kim SY, Woo K, Lim K, Lee K, Jang HS (2013) Highly bright multicolor tunable ultrasmall β-$Na(Y,Gd)F_4$:Ce,Tb,Eu/β-$NaYF_4$ core/shell nanocrystals. Nanoscale 5(19):9255–9263
25. Parchur AK, Prasad AI, Ansari AA, Rai SB, Ningthoujam RS (2012) Luminescence properties of Tb^{3+} doped $CaMoO_4$ nanoparticles: annealing effect, polar medium dispersible, polymer film and core-shell formation. Dalton Trans 41(36):11032–11045
26. Ansari AA, Singh SP, Singh N, Malhotra BD (2012) Synthesis and characterization of silica coated NdF_3 core shell nanoparticles by sol-gel process. Spectrochim Acta Part A 86(9):432–436
27. Gao G, Zhang C, Zhou Z, Zhang X, Ma J, Li C, Jin W, Cui D (2013) One-pot hydrothermal synthesis of lanthanide ions doped one-dimensional upconversion submicrocrystals and their potential application in vivo CT imaging. Nanoscale 5(1):351–362
28. He F, Niu N, Wang L, Xu J, Wang Y, Yang G, Gai S, Yang P (2013) Influence of surfactants on the morphology, upconversion emission, and magnetic properties of β-$NaGdF_4$:Yb^{3+},Ln^{3+} (Ln = Er, Tm, Ho). Dalton Trans 42(27):10019–10028
29. Tauc J, Menth A (1972) States in the gap. J Non-Cryst Solids 8(9): 569–585
30. Wang ZL, Quan ZW, Jia PY, Lin CK, Luo Y, Chen Y, Fang J, Zhou W, O'Connor CJ, Lin J (2006) A facile synthesis and photoluminescent properties of redispersible CeF_3, CeF_3:Tb^{3+}, and CeF_3:Tb^{3+}/LaF_3 (core/shell) nanoparticles. Chem Mater 18(8):2030–2037
31. Liu Y, Chen W, Wang S, Joly AG, Westcott S, Woo BK (2008) X-ray luminescence of LaF_3: Tb^{3+} and LaF_3: Ce^{3+}, Tb^{3+} water-soluble nanoparticles. J Appl Phys 103(6):063105–063105
32. Ansari AA, Parchur AK, Alam M, Labis JP, Azzeer A (2014) Influence of surface coating on structural and photoluminescent properties of $CaMoO_4$:Pr, nanoparticles. J Fluoresc 24(4): 1253–1262
33. Liu T, Xu W, Bai X, Song H (2012) Tunable silica shell and its modification on photoluminescent properties of Y_2O_3:Eu^{3+}@SiO_2 nanocomposites. J Appl Phys 111:064312
34. Singh LR, Ningthoujam RS, Sudarsan V, Srivastava I, Dorendrajit S, Singh DGK, Kulshreshtha SK (2008) Luminescence study on Eu^{3+} doped Y_2O_3nanoparticles: particle size, concentration and core–shell formation effects. Nanotechnology 19(5):055201
35. Luwang MN, Ningthoujam RS, Srivastava SK, Vatsa RK (2011) Preparation of white light emitting YVO_4: Ln^{3+} and silica-coated YVO_4: Ln^{3+}(Ln^{3+} = Eu^{3+}, Dy^{3+}, Tm^{3+}) nanoparticles by CTAB/n-butanol/hexane/water microemulsion route: energy transfer and site symmetry studies. J Mater Chem 21(14):5326–5337
36. Di W, Wang X, Chen B, Lu S, Zhao X (2005) Effect of -OH on the luminescent efficiency and lifetime of Tb^{3+}-doped yttrium orthophosphate synthesized by solution precipitation. J Phys Chem B 109(27):13154–13158
37. Parchur AK, Ningthoujam RS, Rai SB, Okram GS, Singh RA, Tyagi M, Gadkari SC, Tewari R, Vatsa RK (2011) Luminescence properties of Eu^{3+} doped $CaMoO_4$ nanoparticles. Dalton Trans 40(29):7595–7601
38. Li G, Wang Z, Quan Z, Li C, Lin J (2007) Growth of highly crystalline $CaMoO_4$:Tb^{3+} phosphor layers on spherical SiO_2 particles via sol − gel process: structural characterization and luminescent properties. Cryst Growth Des 7(9):1797–1802
39. Stouwdam JW, van Veggel FCJM (2004) Improvement in the luminescence properties and processability of LaF_3/Ln and $LaPO_4$/Ln nanoparticles by surface modification. Langmuir 20(26): 11763–11771